



PHLPP2 is a pseudophosphatase that lost activity in the metazoan ancestor

Tarik Husremović^{a,1}, Vanessa Meier^{a,1}, Lucas Piëch^{a,b}, Katharina M. Siess^a, Sumire Antonioli^{a,b}, Irina Grishkovskaya^c , Nikoleta Kircheva^d, Silvia E. Angelova^{d,e} , Karoline Wenzl^a, Andreas Brandstätter^f , Jiri Veis^a, Fran Miočić-Stošić^{a,b,g}, Dorothea Anrather^{h,i} , Markus Hartl^{h,i} , Linda Truebestein^a, Luis M. Cerron-Alvan^{a,b,j}, Martin Leeb^{a,j}, Bojan Žagrović^{a,g} , Stephan Hann^f , Christoph Bock^{k,l} , Egon Ogris^a , Todor Dudev^m , Nicholas A. T. Irwinⁿ, David Haselbach^c , and Thomas A. Leonard^{a,2}

Affiliations are included on p. 11.

Edited by Wolfgang Peti, UConn Health, Farmington, CT; received August 23, 2024; accepted February 28, 2025 by Editorial Board Member Natalie G. Ahn

The phosphoinositide 3-kinase (PI3K) pathway is a major regulator of cell and organismal growth. Consequently, hyperactivation of PI3K and its downstream effector kinase, Akt, is observed in many human cancers. Pleckstrin homology domain leucine-rich repeat-containing protein phosphatases (PHLPP), two paralogous members of the metal-dependent protein phosphatase family, have been reported as negative regulators of Akt signaling and, therefore, tumor suppressors. However, the stoichiometry and identity of the bound metal ion(s), mechanism of action, and enzymatic specificity of these proteins are not known. Seeking to fill these gaps in our understanding of PHLPP biology, we unexpectedly found that PHLPP2 has no catalytic activity *in vitro*. Instead, we found that PHLPP2 is a pseudophosphatase with a single zinc ion bound in its catalytic center. Furthermore, we found that cancer genomics data do not support the proposed role of PHLPP1 or PHLPP2 as tumor suppressors. Phylogenetic analyses revealed an ancestral phosphatase that arose more than 1,000 Mya, but that lost activity at the base of the metazoan lineage. Surface conservation indicates that while PHLPP2 has lost catalytic activity, it may have retained substrate binding. Finally, using phylogenomics, we identify coevolving genes consistent with a scaffolding role for PHLPP2 on membranes. In summary, our results provide a molecular explanation for the inconclusive results that have hampered research on PHLPP and argue for a focus on the noncatalytic roles of PHLPP1 and PHLPP2.

phosphatase | Akt | PHLPP | signaling | cancer

Cell and organismal growth depend on growth factors that activate receptor tyrosine kinases (RTKs) expressed on the surface of cells. RTK activation leads to the recruitment and activation of the small guanosine triphosphatase (GTPase) Ras and the lipid kinase phosphoinositide 3-kinase (PI3K), which synergistically drive the conversion of phosphatidylinositol-4,5-bisphosphate (PIP₂) in the plasma membrane into the lipid second messenger phosphatidylinositol-3,4,5-trisphosphate (PIP₃). PIP₃, in turn, recruits and activates a number of effector proteins, including the serine/threonine protein kinase Akt and its upstream activator phosphoinositide-dependent kinase 1 (PDK1) (1). PDK1 and Akt control essential aspects of cell growth, proliferation, differentiation, and metabolism, including glucose homeostasis (2). The lipid phosphatase and tumor suppressor, phosphatase and tensin homolog (PTEN), attenuates PI3K signaling by converting PIP₃ back into PIP₂. Mutations in Ras and PI3K, as well as loss of PTEN, are frequently observed in human cancers (3). Akt itself is also found mutated in cancer (4) and the rare overgrowth disorder, *Proteus* syndrome (5).

Akt is an AGC kinase, consisting of a PIP₃-binding pleckstrin homology (PH) domain and a kinase domain which bears two regulatory phosphorylation motifs. PDK1 phosphorylates Akt1 at T308 in its activation loop (6), while mTORC2 is widely believed to phosphorylate S473 in its hydrophobic motif (7). A third phosphorylation site in the C-terminal tail, the turn motif, is constitutively phosphorylated and controls Akt stability (8). Phosphorylation of T308 and S473 promotes disorder-to-order transitions of their respective motifs, leading to Akt activation (9).

PIP₃ turnover by PTEN leads to the dissociation and inactivation of Akt. An important, but poorly understood aspect of Akt inactivation is the dephosphorylation of T308 and S473 by protein phosphatases. T308 is dephosphorylated by protein phosphatase 2A (PP2A) (10, 11), whereas S473 has been reported to be the target of the PH domain leucine-rich repeat-containing protein phosphatases PHLPP1 and PHLPP2 (12, 13). The original identification of PHLPP as an Akt phosphatase was guided by the hypothesis that since S473

Significance

PHLPP1 and PHLPP2 have previously been reported as protein phosphatases that specifically inactivate Akt, a pro-growth and survival kinase hyperactivated in many human cancers. Unexpectedly, we found that purified PHLPP2 has no detectable enzymatic activity *in vitro*. This observation can be rationalized by its unusual active site, which has diverged significantly from that of canonical metal-dependent phosphatases. Furthermore, we show that cancer genomics does not support a role for either PHLPP1 or PHLPP2 in cancer. Our findings argue for the exploration of alternative hypotheses regarding the role of PHLPP in Akt signaling and cancer, with a focus on its non-catalytic functions.

Author contributions: T.H., V.M., L.P., K.M.S., S.A., N.K., S.E.A., D.A., M.H., B.Ž., T.D., N.A.T.I., and T.A.L. designed research; T.H., V.M., L.P., K.M.S., S.A., N.K., S.E.A., K.W., A.B., F.M.-S., D.A., T.D., N.A.T.I., and T.A.L. performed research; J.V., L.T., S.H., and E.O. contributed new reagents/analytic tools; T.H., K.M.S., I.G., N.K., S.E.A., K.W., A.B., F.M.-S., D.A., M.H., L.M.C.-A., M.L., C.B., T.D., N.A.T.I., D.H., and T.A.L. analyzed data; C.B. advised on cancer genomics data analysis; and T.A.L. wrote the paper.

The authors declare no competing interest.

This article is a PNAS Direct Submission. W.P. is a guest editor invited by the Editorial Board.

Copyright © 2025 the Author(s). Published by PNAS. This open access article is distributed under [Creative Commons Attribution License 4.0 \(CC BY\)](https://creativecommons.org/licenses/by/4.0/).

¹T.H. and V.M. contributed equally to this work.

²To whom correspondence may be addressed. Email: thomas.leonard@meduniwien.ac.at.

This article contains supporting information online at <https://www.pnas.org/lookup/suppl/doi:10.1073/pnas.2417218122/-/DCSupplemental>.

Published April 1, 2025.

phosphorylation is growth factor or serum-sensitive, such a phosphatase might contain a PH domain. The PH domain would presumably target it to the same membranes where Akt is activated (12). While PHLPP1 and PHLPP2 double knockout mice exhibit only a mild colitis resistance phenotype (14), their proposed repressive effects on Akt signaling have led to their designation as tumor suppressor genes (12, 15, 16). However, the mechanisms by which these phosphatases target Akt for dephosphorylation and the structural basis for their specificity are currently unknown.

Here, we show that—in contrast to previous reports—PHLPP2 is actually a pseudophosphatase. We show that PHLPP2 has a divergent catalytic site, exhibits no activity *in vitro*, and that cancer genomics does not support a role for either PHLPP1 or PHLPP2 in cancer. We corroborate the absence of phosphatase activity by showing that PHLPP evolved from an ancestral phosphatase that lost activity in the metazoan ancestor. Our findings refute the notion that PHLPP is an Akt phosphatase and question efforts to pharmacologically target PHLPP activity (15, 17). Finally, we establish a molecular and evolutionary basis for reassessing the biological roles of PHLPP1 and PHLPP2 as membrane-associated scaffold proteins.

Results

PHLPP2 Exhibits No Detectable Activity against Akt. We expressed GST-tagged, full-length human PHLPP2 in baculovirus-infected Sf9 insect cells and purified it to homogeneity by sequential affinity, ion exchange, and size-exclusion chromatography (*SI Appendix, Fig. S1A*). PHLPP2 was confirmed to be predominantly monomeric by mass photometry (*SI Appendix, Fig. S1B*) and the masses of all recombinant PHLPP2 constructs were verified by denaturing mass spectrometry (*SI Appendix, Fig. S1 C–E*). PHLPP2 and all mutants were confirmed to be properly folded by analytical size-exclusion chromatography (*SI Appendix, Fig. S1F*) and thermal stability assays (*SI Appendix, Fig. S1G*). Addition of EDTA to PHLPP2 did not affect its global thermal stability (*SI Appendix, Fig. S1G*).

Akt has been reported as a substrate of both PHLPP1 and PHLPP2 in mammalian cells (12, 13, 18). Fig. 1*A* shows the structure of the kinase domain of Akt alongside the sequence motifs of its activation loop and hydrophobic motif. According to reports, PHLPP is specific for the hydrophobic motif (pS473). To test the activity of recombinant PHLPP2 against synthetic Akt phosphopeptides, we monitored phosphate production in a malachite green assay (MGA). As a control, we assayed a mutant of PHLPP2 (D1024N) (*SI Appendix, Fig. S1E*), designed to abrogate catalytic activity (18). Unexpectedly, PHLPP2^{D1024N} exhibited comparable activity to wild-type PHLPP2 against the Akt1 activation loop peptide (Fig. 1*B*). When assayed against both the activation loop and hydrophobic motif peptides, we detected very low, but variable activity from multiple independent preparations of wild-type PHLPP2. This activity, however, was entirely lost upon treatment of each preparation with 12.5 nM okadaic acid (Fig. 1 *C* and *D*), a highly specific PP2A/PP4/PP6 inhibitor and toxin produced by several species of dinoflagellate (19, 20). Since previous reports have implicated PP2A in Akt1 dephosphorylation (10, 11, 21), we suspected contamination of purified PHLPP2 with PP2A. As a control, we assayed the activity of recombinant PP2A against both peptides, which exhibited a specific activity 50-fold greater than any of our PHLPP2 preparations (Fig. 1 *E* and *F*). Inhibition of all phosphatase activity in our PHLPP2 assays occurred despite PHLPP2 being present in molar excess over okadaic acid in all but one concentration. Finally, PHLPP2 exhibited no activity against either pT308 or pS473 of stoichiometrically phosphorylated full-length Akt1 (prepared according

to ref. 22) under the assay conditions of the study that reported phosphatase activity of PHLPP for the first time (12) (*SI Appendix, Fig. S2 A–C*).

Suspecting that recombinant PHLPP2 preparations may be contaminated with one or more phosphatases of the PP2A family, we subjected purified PHLPP2 to peptide fingerprinting mass spectrometry. While PHLPP2 was estimated to be more than 99.9% pure, peptides of all three subunits of *Spodoptera frugiperda* PP2A were detected (Fig. 1*G*). A total of 13 unique peptides corresponding to the PP2A catalytic (C) subunit (2), A-subunit (9), and B55 (B) regulatory subunit (2) were measured. With a mass of 157 kDa, the PP2A heterotrimer is very close in mass to PHLPP2 (147 kDa), such that they cannot be separated by size-exclusion chromatography. The identification of PP2A holoenzymes in recombinant PHLPP2 preparations explains the okadaic acid sensitivity of the observed phosphatase activity (Fig. 1 *C* and *D*).

To assess whether contaminating phosphatase activity may have been the source of literature reports of PHLPP activity, we immunoprecipitated ectopically expressed V5-tagged PHLPP2 from HEK293 cells using V5 nanobody-conjugated magnetic beads and subjected the beads to a series of successive wash steps, while measuring phosphatase activity at each step in the absence and presence of okadaic acid (Fig. 1*H*). We observed that all of the measurable phosphatase could be successively washed away while keeping PHLPP2 constant, and that any residual activity could be inhibited by okadaic acid (Fig. 1*I* and *SI Appendix, Fig. S2D*).

The absence of phosphatase activity in PHLPP2 immunoprecipitated from mammalian cells suggested that PHLPP2 may not, in fact, attenuate Akt signaling. To address this directly, we generated PHLPP2 knockout HEK293 cells by CRISPR/Cas9 (*SI Appendix, Fig. S3 A and B*) and subjected them to transcriptomics analysis by RNAseq. Akt directly phosphorylates transcription factors of the FoxO family, leading to their sequestration in the nucleus by 14-3-3 proteins and consequent changes in the transcription of FoxO-activated genes (23). Deletion of PHLPP2 in HEK293 cells resulted in a significant deregulation of 641 genes (adj. $P \leq 0.05$; *SI Appendix, Fig. S3C* and Table S2). These genes were significantly enriched in RNA regulation and transcription, but no functional enrichment directly related to Akt activity was detected. Further supporting a role independent of the regulation of Akt, we could not detect a significant preferential deregulation of reported FOXO1 target genes in PHLPP2 KO cells (*SI Appendix, Fig. S3 D–G*) (24, 25).

PHLPP2 Is a Pseudophosphatase. To confirm that the activity detectable in our purified PHLPP2 came from contaminating PP2A, we modified our purification protocol to include the reverse affinity-based removal of PP2A. Produced by the cyanobacterium, *Microcystis aeruginosa*, microcystin-LR is a high-affinity irreversible inhibitor of PP1, PP2A, PP3, PP4, and PP6 phosphatases that forms a covalent bond to PP2A C269 (Fig. 2*A*) and binds to PP2A in the same binding site as okadaic acid (Fig. 2*B*) (20). Microcystin-LR can be covalently coupled to sepharose beads to create phosphatase inhibitor beads (PIBs, Fig. 2*C*) (26). We confirmed that our PIBs were highly effective in enriching PP2A from PHLPP2-expressing Sf9 cell lysates by label-free quantitative mass spectrometry (Fig. 2*D*). As a control, we treated an equivalent lysate with 500 nM okadaic acid to inhibit all okadaic acid-sensitive phosphatases. Since okadaic acid and microcystin-LR bind to the same pocket, PIBs should not enrich these phosphatases in the okadaic acid-treated control. Mass spectrometry analysis confirmed a 1,200-, 540-, and 65-fold enrichment of the PP2A C, A, and B subunits respectively. The three most enriched proteins

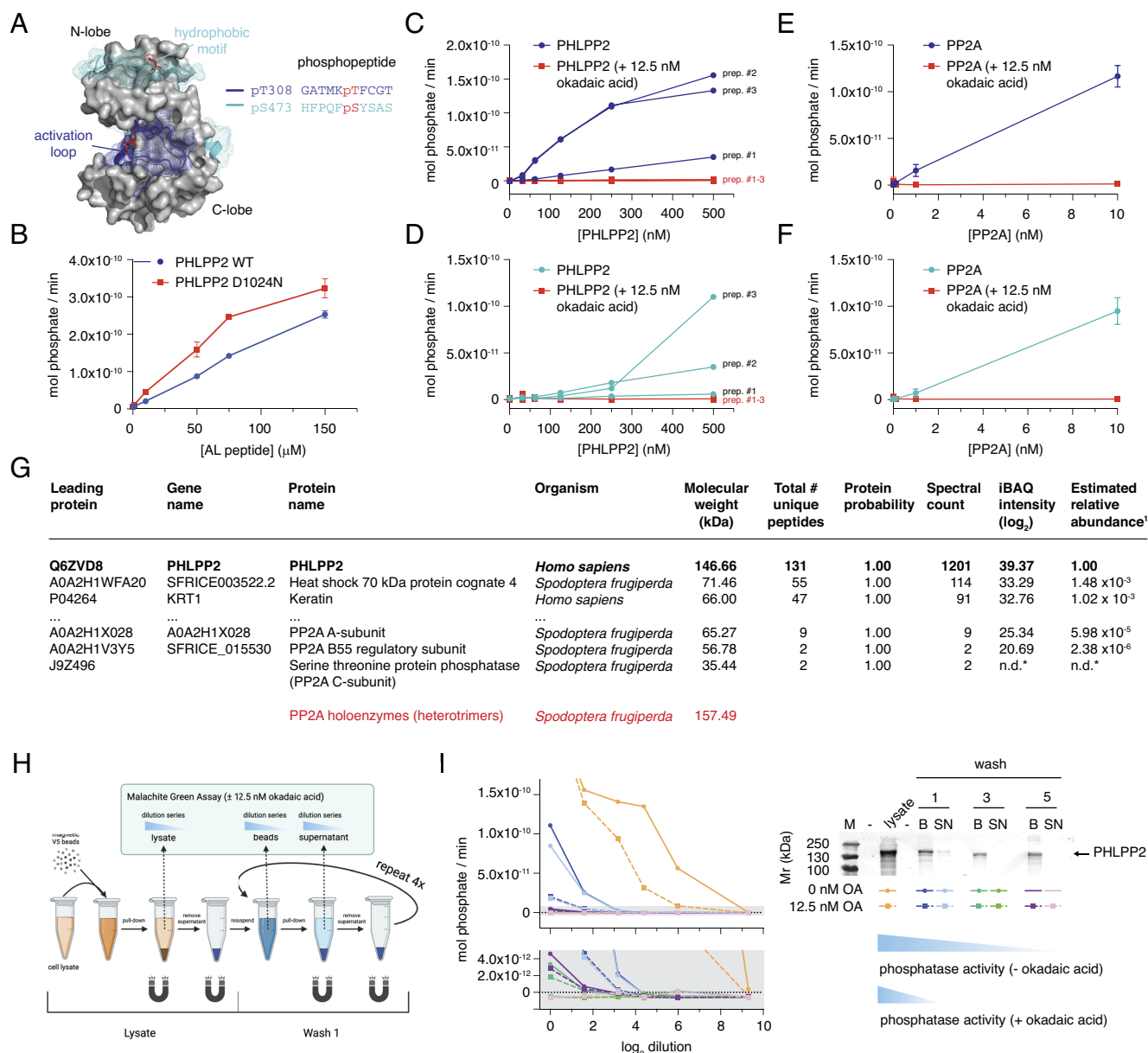


Fig. 1. PHLPP2 exhibits no detectable activity against Akt. (A) Structure of the Akt1 kinase domain depicting activation loop (T308, blue) and hydrophobic motif (S473, cyan) phosphopeptides used in phosphatase assays. (B) Protein phosphatase activity of purified PHLPP2^{D1024N} (red) compared to PHLPP2^{WT} (blue) against the activation loop peptide of Akt. (C) Dephosphorylation of the activation loop peptide by three independent preparations of recombinant PHLPP2 purified from Sf9 insect cells (blue) ±12.5 nM okadaic acid (red). (D) Dephosphorylation of the hydrophobic motif peptide by three independent preparations of recombinant PHLPP2 purified from Sf9 insect cells (cyan) ±12.5 nM okadaic acid (red). (E) Dephosphorylation of the activation loop peptide by purified PP2A (blue) ±12.5 nM okadaic acid (red). (F) Dephosphorylation of the hydrophobic motif peptide by purified PP2A (cyan) ±12.5 nM okadaic acid (red). (G) Peptide fingerprinting mass spectrometry to identify proteins in recombinant PHLPP2 purified from insect cells. Red: molecular weight of Sf9 PP2A heterotrimers. (H) Schematic for immunoprecipitation of PHLPP2 from HEK293 cells and subsequent phosphatase assay. (I) Phosphatase activity of immunoprecipitated PHLPP2 determined after successive wash steps ±12.5 nM okadaic acid. B = beads, SN = supernatant.

correspond to the same three contaminating PP2A proteins observed in PHLPP2 preparations (Fig. 2D and SI Appendix, Fig. S4). Importantly, recombinant PHLPP2 was not observed to be enriched over the control lysate (Fig. 2D).

To remove contaminating PP2A from PHLPP2, we incubated the purified protein with PIBs following anion exchange chromatography and prior to size-exclusion chromatography (Fig. 2E). PIB-treated PHLPP2 lost all detectable activity against both Akt phosphopeptides (Fig. 2F), even at concentrations 500-fold above its known physiological concentration (27). Finally, we evaluated the capacity of PHLPP2 to dephosphorylate *para*-nitrophenyl phosphate (pNPP). PHLPP2 that had been purified via the scheme shown in Fig. 2E exhibited no activity against pNPP even

in the absence of okadaic acid (Fig. 2G). As a positive control, pNPP was robustly dephosphorylated by lambda phosphatase under the same conditions (Fig. 2G). Importantly, since lambda phosphatase depends on manganese ions for its activity (28), which is also the case for PP2C family phosphatases (29, 30), this experiment explicitly rules out that PHLPP2 exhibits activity in the presence of millimolar concentrations of manganese. In summary, we were unable to detect any phosphatase activity associated with purified, PP2A-free PHLPP2.

The lack of PHLPP2 activity immediately begs the question of which phosphatase dephosphorylates and, thereby, inactivates Akt in cells. To assess the capacity of PP2A holoenzymes to dephosphorylate Akt1, we generated knockouts of the PP2A regulatory

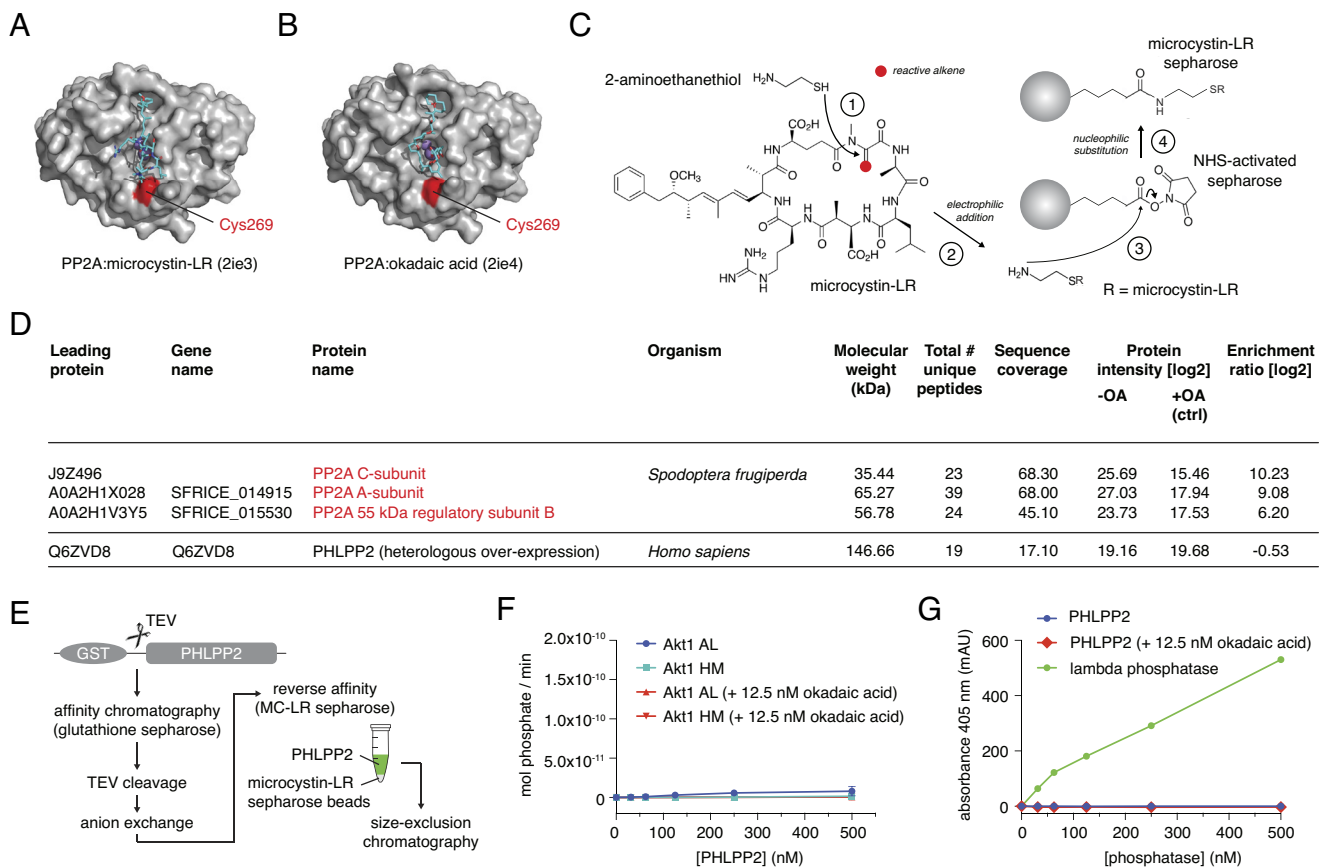


Fig. 2. PHLPP2 is a pseudophosphatase. (A) Structure of the PP2A catalytic subunit bound to the covalent inhibitor microcystin-LR. (B) Structure of the PP2A catalytic subunit bound to okadaic acid. (C) Schematic for covalently coupling microcystin-LR to NHS-activated sepharose beads (26). (D) Tandem mass spectrometry analysis of proteins bound to microcystin-LR-conjugated beads after incubation with cell lysates of Sf9 cells heterologously overexpressing PHLPP2. (E) Purification scheme for affinity-based removal of PP2A family phosphatases from purified PHLPP2. (F) Dephosphorylation of activation loop (blue) and hydrophobic motif (cyan) peptides by PHLPP2 purified according to the scheme in $E \pm 12.5$ nM okadaic acid (red). (G) Dephosphorylation of the generic phosphatase substrate para-nitrophenyl phosphate (pNPP, blue) by PHLPP2 purified according to the scheme in $E \pm 12.5$ nM okadaic acid (red) or lambda phosphatase (green). Assay buffer includes 2 mM $MnCl_2$.

subunits B56 α , B56 β , B56 ϵ , and a double knockout of B56 α/ϵ in HAP1 cells. We compared the phosphorylation state of Akt1 T308 and S473 to wild-type HAP1 cells, including okadaic acid as a control. Knocking out the B56 β subunit of PP2A led to a significant increase in Akt1 phosphorylation on both T308 and S473, while inhibition of all PP2A, PP4, and PP6 enzymes with okadaic acid led to a dramatic increase in Akt1 phosphorylation (SI Appendix, Fig. S5 A–D). These observations indicate that the PP2A B56 β phosphatase is primarily responsible for Akt dephosphorylation in cells.

PHLPP2 is a Zinc-Binding Protein with Altered Metal Ion Stoichiometry. Members of the metal-dependent family of protein phosphatases (PPM), exemplified by protein phosphatase Mg^{2+}/Mn^{2+} -dependent (PPM1A), depend on two or three divalent metal ions in their active site for catalysis (29–31) (Fig. 3A). PHLPP1 and PHLPP2, however, exhibit poor conservation of a number of key residues required for metal ion coordination (Fig. 3B).

To investigate whether the metal ion-binding properties of PHLPP2 could explain the lack of catalytic activity, we determined the identity and stoichiometry of any metal ions copurifying with PHLPP2 by size-exclusion chromatography coupled to inductively coupled plasma mass spectrometry (SEC-ICP-MS). This analysis revealed a single zinc ion in three independent preparations of the protein (Fig. 3C and D and SI Appendix, Fig. S6 A and B). No signal for iron, copper, manganese, or calcium was detected (Fig. 3C).

Using the AlphaFold2-predicted structure of the phosphatase domain, which superimposes on the experimentally determined structure of PPM1A with a rmsd of 1.09 Å, the most likely constellation of zinc-coordinating residues was identified as C799, D820, D822, and D1024, which correspond to the M2 metal ion binding site (SI Appendix, Fig. S6C). The crystal structure of the related pseudophosphatase, [Transforming growth factor β -activated kinase 1]-binding protein 1 (TAB1), also revealed a single manganese ion in the M2 site (33) (SI Appendix, Fig. S6D). The M1 and M3 binding sites can be excluded on the basis of a lack of conservation of suitable residues at these positions. All four putative Zn^{2+} -coordinating residues (C799, D820, D822, and D1024) are invariant in chordate PHLPP1 and PHLPP2 genes (Fig. 3B). No other candidate cysteine, histidine, aspartate, or glutamate residues exist in the vicinity of the M2 site.

To determine experimentally whether C799 was a coordinating ligand of the zinc ion, we alkylated purified PHLPP2 under native conditions with iodoacetamide (IAA), followed by methyl methanethiosulfonate (MMTS) under denaturing conditions (Fig. 3E) and analyzed the peptides by tandem mass spectrometry (Fig. 3F and SI Appendix, Fig. S6E). C467 and C690 exhibited very high ratios of MMTS- to IAA-modified peptides, consistent with them being buried in the hydrophobic core of the LRR domain. Conversely, residues in the intrinsically disordered C-terminal tail all exhibited very low ratios, consistent with high solvent accessibility. C799, though predicted to be solvent exposed, exhibited a high MMTS to IAA ratio, indicating that it is protected from

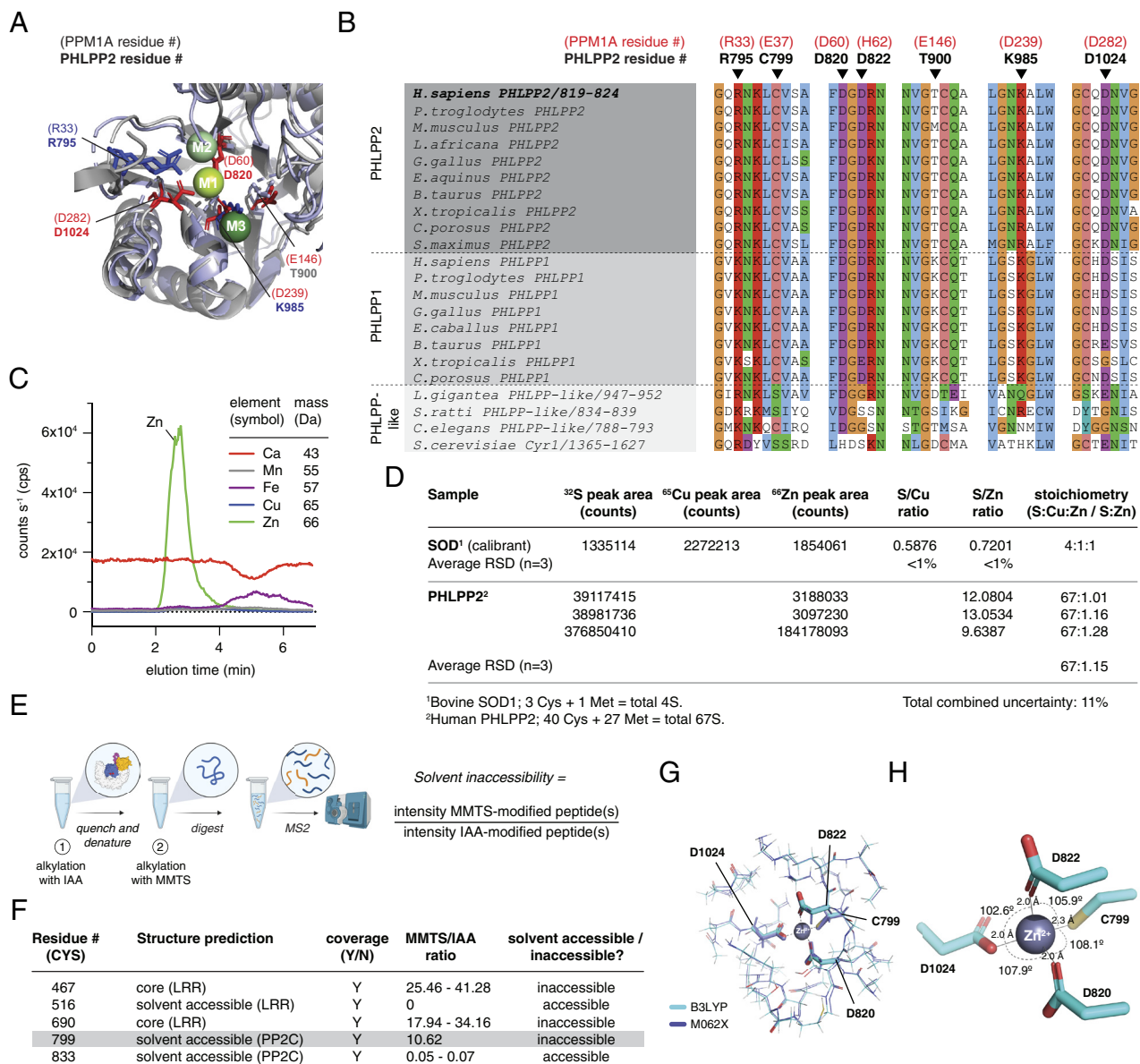


Fig. 3. PHLPP2 is a zinc-binding protein. (A) Catalytic site of PPM1A phosphatase (gray) superimposed on the AF2 model of the PHLPP2 PP2C domain (lilac). M1, M2, and M3 metal ions shown in spheres; metal coordinating amino acids shown in stick representation. PPM1A residue numbers shown in parentheses. (B) Multiple sequence alignment of the metal ion-coordinating motifs of PHLPP1, PHLPP2, and PHLPP-like proteins across a wide evolutionary time. PPM1A residue numbers shown above the alignment in parentheses. (C) ICP-MS chromatograms for recombinant human PHLPP2. (D) Calibration of PHLPP2:Zn²⁺ stoichiometry for three biological replicates. (E) Differential alkylation of PHLPP2 under native and denaturing conditions, coupled to mass spectrometry. (F) Differential alkylation of five different peptides of PHLPP2 (two representing buried cysteines, 2 representing surface exposed cysteines, and one encompassing C799). (G) Quantum mechanical simulation of zinc ion coordination sphere using the ONIOM method (32). Results of two quantum mechanical frameworks (B3LYP and M062X) are shown. (H) Geometry of the zinc-binding site from the simulations showing bond angles and lengths.

alkylation under native conditions. We therefore concluded that C799, in the M2 binding site, coordinates the single zinc ion that copurifies with PHLPP2.

To obtain a reasonable starting structure for the bound zinc ion, we performed explicit-solvent molecular dynamics (MD) simulations starting from the predicted PHLPP2 structure and using distance restraints between the ion and the coordinating atoms obtained from the structure of the C1D3 zinc finger of α -klotho (32). During the simulations, the global atom-positional rmsd with respect to the initially equilibrated structure reached a stable level of 0.2 to 0.25 nm after 10 ns, indicating that placement of the zinc ion in the M2 site is compatible with the folded conformation of the PP2C domain (SI Appendix, Fig. S6F). Since MD is not capable of modeling the electronic environment with sufficient accuracy, we modeled the binding site using the ONIOM

approach (34). Here, atoms three bonds away from the zinc ion were treated quantum-mechanically, while atoms further away were treated semiempirically. To validate the ONIOM method, we simulated the zinc-binding site of α -klotho (32). The best scoring models of the zinc-binding site obtained from two quantum mechanical frameworks exhibited near tetrahedral geometry and bond lengths consistent with experimentally determined zinc clusters (Fig. 3 G and H and SI Appendix, Fig. S6 G and H). The free energy change associated with substitution of zinc for either manganese (Mn²⁺) or iron (Fe²⁺) was 7 to 12 kcal/mol (SI Appendix, Fig. S6I), indicating that the binding site is energetically optimized for zinc.

Since all known PPM family phosphatases require a minimum of two metal ions (M1 and M2) for catalytic activity, the absence of PHLPP2 activity can be explained.

Cancer Genomics Does Not Support a Role for PHLPP1 or PHLPP2 as Tumor Suppressors. Since we could not measure any detectable phosphatase activity of PHLPP2, we investigated the evidence for the role of PHLPP1 or PHLPP2 as tumor suppressors. Akt1, Akt2, and Akt3 are all established oncogenes with gain-of-function (GOF) mutational hotspots (4, 35) (Fig. 4A). To assess somatic mutations in either PHLPP1 or PHLPP2 associated with cancer, we plotted synonymous (silent) and nonsynonymous (missense) mutations reported in the Catalog of Somatic Mutations In Cancer (COSMIC) database (36) and compared them to two Cancer Gene Census (CGC) (35) tumor suppressor genes, two CGC oncogenes, and two randomly chosen olfactory receptor genes as negative controls (genes that are very unlikely to be functionally involved in cancer development). Fig. 4B shows that the rate of both synonymous and nonsynonymous mutations in *PHLPP1* and *PHLPP2* is comparable to those of the olfactory receptor genes *OR2A4* and *OR51E2*, while the rates of nonsynonymous mutations in both *PTEN* and *TP53*, as well as *KRAS* and *BRAF*, are significantly higher in human cancers. As expected, nonsynonymous loss-of-function (LOF) mutations are significantly enriched at hotspots (red) known to disrupt the function of *PTEN* and *TP53* tumor suppressor genes, while GOF mutations are enriched in *KRAS* and *BRAF* oncogenes (Fig. 4C). In contrast, *PHLPP1* and *PHLPP2* show comparable rates of nonsynonymous mutations to *OR2A4* and *OR51E2* throughout their coding regions. To determine whether copy number variants (CNVs) are significantly enriched in human cancers, we plotted copy number losses (CNL) and gains (CNG) for each of the genes in Fig. 4B. *PTEN* and *TP53* exhibit a high frequency of CNL (red) consistent with their tumor suppressive function, while *KRAS* and

BRAF exhibit a high frequency of CNG (green) consistent with their oncogenic potential (Fig. 4D). In contrast, *PHLPP1* and *PHLPP2* show comparable rates of CNVs to *OR2A4* and *OR51E2*.

To assess whether PHLPP1 or PHLPP2 is an essential gene in cancer cells, we plotted the gene effect score for 1,100 cancer cell lines reported in the Dependency Map (DepMap) Public 23Q4+Score (Chronos) CRISPR knockout screens (37–40), 710 cancer cell lines reported in the Achilles+DRIVE+Marcotte (DEMETER2) RNA interference (RNAi) knockdown screens (41–44), and 317 cancer cell lines reported in copy number effect-corrected (39) CRISPR knockout screens (SI Appendix, Fig. S7 A and B). Neither PHLPP1 nor PHLPP2 were found to be essential in any of these screens. These observations are consistent with the viability of single knockout mice for both PHLPP1 (45, 46) and PHLPP2 (14), as well as a *PHLPP1*^{−/−} *PHLPP2*^{−/−} double knockout mouse (14), none of which have been reported to exhibit a significantly higher propensity to develop tumors.

Finally, we mapped the results of genome-wide association studies (GWAS) for the genetic loci of *PHLPP1* and *PHLPP2*. An intron variant in the neighboring *BCL2* gene has been associated with prostate carcinoma in two GWASs with *P*-values < 5.0×10^{-8} (47, 48), but no cancer associations have been reported for either *PHLPP1* or *PHLPP2* (SI Appendix, Fig. S7 C and D). Analysis of synthetic lethal screens of cancer cells also found no evidence for synthetic lethal interactions involving either PHLPP1 or PHLPP2 (49). In summary, there is scant evidence from disease genotypes, clinically reported variants, or GWASs to support that dysregulation of either PHLPP1 or PHLPP2 is associated with cancer.

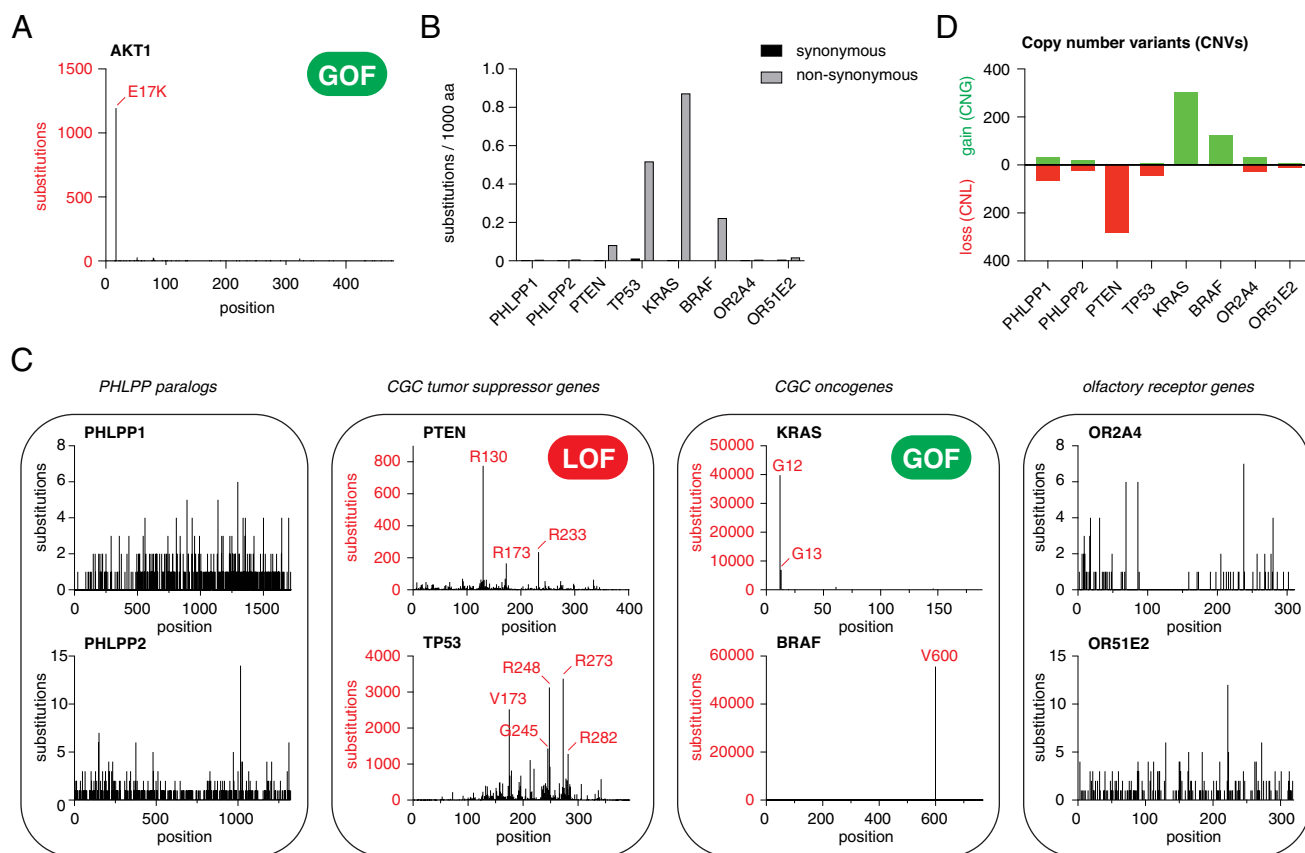


Fig. 4. Cancer genomics does not support a role of PHLPP1 or PHLPP2 as tumor suppressors. (A) Distribution of nonsynonymous mutations within the coding sequence of Akt1 (Tier 1 Cancer Gene Census cancer gene). Red: known hotspot mutations. (B) Number of synonymous and nonsynonymous substitutions per 1,000 amino acids reported in COSMIC for: PHLPP1 and PHLPP2; the tumor suppressor genes PTEN and TP53; the oncogenes KRAS and BRAF; the olfactory receptor genes OR2A4 and OR51E2. (C) Distribution of nonsynonymous mutations within the coding sequence of the genes represented in (A). Red: known hotspot mutations in CGC genes. (D) CNV for the genes represented in (B). Green: CNG; red: CNL.

PHLPP2 Exhibits a Conserved Arrangement of Its Regulatory Domains.

Both PHLPP1 and PHLPP2 comprise an N-terminal Ras-associated (RA) domain followed by a PH domain, an LRR domain, and a C-terminal protein phosphatase 2C (PP2C) domain (Fig. 5*A*). Rotary shadowing electron microscopy revealed particles with a regular horseshoe-shaped conformation (Fig. 5*B*, *Inset*) consistent with the AlphaFold2-predicted structure of PHLPP2 (Fig. 5*C* and *D*). We next determined the structure of PHLPP2 by single-particle cryoelectron microscopy (cryoEM). We obtained two distinct reconstructions from the sample (see *SI Appendix*, Fig. S8 for sample micrographs, 2D class averages, and Fourier Shell Correlation curves). We interpret these as endpoints of a conformational continuum, which explains why the resolution of both maps is limited to 6 Å. The two conformations differ in the location of the PH domain, which appears to be very flexible and is the least resolved part of the structure. Furthermore, the LRR exhibits bending while the PP2C and RA domains show compaction, potentially changing the accessibility of the phosphatase domain. Nevertheless, the AlphaFold2 prediction of PHLPP2 fits well into the particle volumes for both conformations (Fig. 5*E* and *F*).

Evolution and Diversification of PHLPP Genes. To provide clues to PHLPP function, we used phylogenetics to reconstruct the evolutionary history of the PHLPP protein family. The presence of PHLPP homologs in distantly related eukaryotes such as amoebozoans and parabasalids, suggests that the PHLPP family emerged early in eukaryotic evolution, presumably following the fusion of an LRR protein with a PP2C family phosphatase (Fig. 6*A* and *B*). The ancestral gene encoded all residues known to be required for catalytic activity, including coordination of the

M1 and M2 metal ions (Fig. 6*C* and *D*). To confirm that the evolutionary ancestor of PHLPP was a bona fide phosphatase, we expressed and purified recombinant PHLPP-related LRR-PP2C phosphatase from the amoebozoan *Stenamoeba stenapodia* (SsLRR-PP2C). The correct mass of the recombinant protein was confirmed by mass spectrometry and mass photometry (*SI Appendix*, Fig. S9*A* and *B*). As predicted, SsLRR-PP2C exhibited concentration-dependent phosphatase activity which was insensitive to okadaic acid and completely abrogated by divalent metal ion chelation (Fig. 6*E*).

In the last common ancestor of opisthokonts (e.g., animals and fungi), around 1,000 Mya, the ancestral LRR-PP2C gene gained an RA domain and was subsequently duplicated. Shortly thereafter, one copy of the gene gained a PH and a kinase domain, giving rise to the PHLPP family, whereas the other paralog gained a class III adenylate cyclase (AC), resulting in the emergence of the Cyr1 family (Fig. 6*B*). Retention of PHLPP and Cyr1 in unicellular holozoans [$P = 4.56 \times 10^{-5}$, $\Delta \log\text{-likelihood} = 114.7$, approximately unbiased (AU) test for monophyly], the closest unicellular relatives of animals, indicates that this duplication was followed by reciprocal loss of Cyr1 in metazoa and PHLPP in fungi. The ancestral Cyr1 was likely a pseudophosphatase given the lack of catalytic residues, but it later acquired a dimerization domain in fungi (Fig. 6*A–C*). This contrasts with PHLPP, which only lost its active site in metazoans. Indeed, PHLPP homologs in unicellular holozoans not only encode active site residues, but in some cases include a C-terminal kinase domain (Fig. 6*A–C*). Nonetheless, PHLPP was conserved throughout animal evolution before giving rise to PHLPP1 and PHLPP2 following a duplication event in the common ancestor of vertebrates or gnathostomes. To better understand the impact of these evolutionary changes on PHLPP structure, we

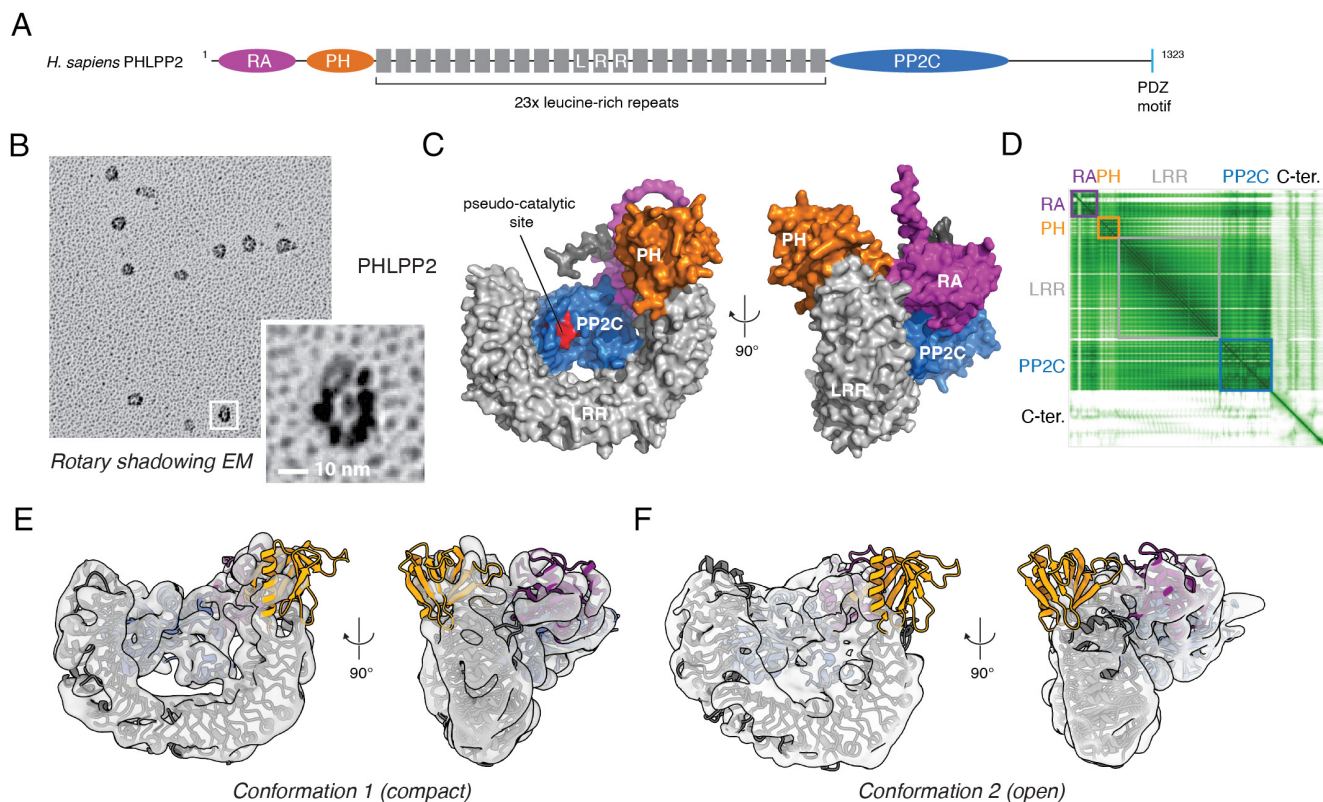


Fig. 5. PHLPP exhibits a conserved arrangement of its regulatory domains. (A) Domain architecture of human PHLPP2 [RA domain, magenta; PH domain, orange; LRR (gray); PP2C, blue; pseudo-catalytic site of PP2C domain, red]. (B) Rotary shadowing electron microscopy of recombinant PHLPP2. (C) Top-ranked AlphaFold2 model of human PHLPP2 [putative active site of PP2C domain, red]. (D) Predicted alignment error (PAE) plot for AF2 prediction in (C). PHLPP2 domain boundaries are indicated by colored boxes. (E) CryoEM maps of human PHLPP2 (conformation 1) at 6 Å resolution with the AlphaFold2-predicted structure of PHLPP2 fit to the map. (F) CryoEM maps of human PHLPP2 (conformation 2) at 6 Å resolution with the AlphaFold2-predicted structure of PHLPP2 fit to the map.

employed AlphaFold2 to predict the three-dimensional structures of representative proteins from across the LRR-PP2C phylogeny. The LRR-PP2C phosphatase of *Entamoeba* is structurally consistent with each of the evolutionarily descended derivatives, including vertebrate PHLPP1 and PHLPP2 and fungal Cyr1 (Fig. 6F). Together, these data suggest that PHLPP emerged through a complex history of neo- and subfunctionalization, based on a conserved LRR-PP2C chassis which repeatedly lost phosphatase activity, including at the origin of animals.

The structure and function of Cyr1 provide a useful comparison when considering the functional diversification of PHLPP. The acquisition of an RA domain, which preceded gene duplication at the base of the opisthokont clade, apparently gave rise to a Ras-dependent functionality in fungal Cyr1. *Saccharomyces cerevisiae* Cyr1 AC activity is stimulated by GTP-bound RAS1 or RAS2 (51), homologs of human KRAS. AlphaFold2 prediction of the RAS1/2:Cyr1 interaction converges on five identical models of very high confidence (SI Appendix, Fig. S9C) that are superimposable with experimentally determined structures of KRAS in complex with RA domains from AF6 (52) and RGL1 (53) (SI Appendix, Fig. S9D).

Reconstitution of yeast Cyr1 AC activity in the heterologous host *Escherichia coli* implies that Cyr1 and RAS are necessary and sufficient for cAMP production (51). Since RAS binding to the RA domain of Cyr1 is not predicted to induce any conformational change in the RA domain, an allosteric mechanism can, most likely, be ruled out. Class III ACs, of which Cyr1 is a member, depend on the homo-, hetero-, or pseudodimerization of two cyclase domains for cAMP production (54). Farnesylation of RAS is essential for Cyr1 activation (55), suggesting that RAS.GTP-dependent recruitment of Cyr1 to the plasma membrane may drive dimerization of the Cyr1 AC domain. AlphaFold2 prediction of a putative dimer of full-length Cyr1 converges on near-identical models (SI Appendix, Fig. S9E) in which the C-terminal ~400 amino acids exhibit a dimeric arrangement (SI Appendix, Fig. S9F) superimposable with the AC domains of Cya (SI Appendix, Fig. S9G), a bacterial AC, the structure of which has been experimentally determined by cryoelectron microscopy (56).

The C-terminal domain (CTD) predicted to dimerize Cyr1 has been reported to bind cyclase-associated protein (CAP), a multidomain protein which links Cyr1 to the actin cytoskeleton (57). Biochemical studies have narrowed down the region of CAP essential for Cyr1 binding to the N-terminal 36 amino acids (58). AlphaFold2 prediction of the complex between the CTD of Cyr1 and CAP converges on 5 identical and high-confidence models in which the dimeric CTD binds the N-terminal helix of CAP in a heterotetrameric arrangement (SI Appendix, Fig. S9H). This model therefore reconciles the mode and stoichiometry of binding of CAP to Cyr1. By combining the predicted models of interaction of Cyr1, RAS, and CAP, a high-confidence prediction of a Cyr1-RAS-CAP heterohexamer (2:2:2) can be obtained (SI Appendix, Fig. S9I).

Similar to Cyr1, acquisition of a PH domain in the PHLPP family appears to have coincided with C-terminal neofunctionalization through the emergence of a kinase domain. Curiously, phylogenetics suggests that this domain belongs to the AGC kinase family, which includes AKT and protein kinase C, another previously proposed target of PHLPP (SI Appendix, Fig. S9J) (59). Like the AC of Cyr1, this kinase domain was appended to the PHLPP C-terminus and may be positionally flexible, as indicated by AlphaFold2 predicted alignment error (PAE) plots (Fig. 6F). The kinase domain was subsequently lost in the metazoan ancestor, concurrently with the phosphatase active site. The functional implications of this domain remain unclear, but could imply an ancestral connection between PHLPP and AGC kinases.

PHLPP May Have an Alternative Scaffolding Role on Membranes.

Despite the apparent pseudogenization of PHLPP, surface conservation maps of vertebrate PHLPP indicate two regions of high conservation: one on the surface of the PH domain and one corresponding to an ~50 amino acid insertion in the PP2C domain (Fig. 7A). Importantly, while the RA domain has been retained in vertebrate PHLPP, its binding to RAS has not. In fact, the surface of the RA domain used by Cyr1 to bind RAS exhibits the highest sequence divergence of any region in PHLPP1 and PHLPP2 (Fig. 7A). The acquisition of a PH domain may have substituted for RAS binding, although in the unicellular holozoan, *Corallichytrium limacisporum*, the PH domain appears to have been lost (Fig. 6A), suggesting a period of functional redundancy. Electrostatic surface potential analysis of PHLPP2 indicates a basic surface overlapping with the binding sites of phosphoinositides in structural homologs of the PH domain (60, 61) (Fig. 7B), suggesting a role for PHLPP at cellular membranes. Consistent with this hypothesis, PHLPP2 exhibited strong binding to phosphoinositides (PIs) in a protein-lipid overlay assay, with a preference for monophosphorylated PIs, particularly PI(4)P (Fig. 7C). Surface conservation within the LRR-PP2C cradle is coincident with an insertion between strands $\beta 7$ and $\beta 8$ of the PP2C domain called the FLAP subdomain (62) that is known to be important for substrate binding in PP2C phosphatases from bacteria (63) to higher eukaryotes (64). PP2C phosphatases found in *Desulfobacteria* exhibit homologous FLAP domains to PHLPP2 (Fig. 7D), suggesting that the evolutionary ancestor of the PHLPP2 PP2C domain may have originated in bacteria. These observations imply that vertebrate PHLPP lost phosphatase activity, but may have retained substrate binding.

To identify proteins associated with PHLPP2, we examined the distribution of PHLPP paralogs across the gnathostome phylogeny. Despite its presumed role in AKT and PKC regulation, PHLPP2 has been lost in at least four animal lineages, including twice independently in turtles, the squamata (snakes and lizards), and caecilians (Fig. 7E). Notably, these losses occurred despite the retention of AKT and PKC orthologs. To identify alternative coevolving genes, we used phylogenomic profiling, which revealed six genes with correlated distributions (Fig. 7E). While these genes lack clear functional connections to PHLPP2, many are membrane associated or secreted, suggesting the possibility of alternative, AKT-independent functional interactions at the membrane.

Discussion

PHLPP2 Is a Pseudophosphatase. We show that purified full-length PHLPP2 exhibits no detectable activity in vitro against either T308 or S473 of Akt, as well as the generic substrate pNPP, even at concentrations 500-fold higher than that found in the cell and at substrate concentrations >1,500-fold higher. This contrasts with the evolutionary ancestor of PHLPP, which exhibits robust metal-dependent, but okadaic acid-insensitive, activity. Our identification of contaminating PP2A in preparations of recombinant PHLPP2 highlights the need for more stringent purification conditions than have previously been employed in order to make confident assessments of the biochemical activity of PHLPP proteins.

Phosphatases of the PPM family catalyze hydrolysis of phosphorylated serine or threonine residues by virtue of a binuclear catalytic site in which two manganese ions are coordinated by a combination of aspartate side chains and ordered water molecules (30). A bridging water molecule coordinated by both Mn^{2+} ions is poised for nucleophilic attack on the substrate phosphate (29, 30) and the M2 metal ion determines the rate-limiting step in substrate hydrolysis (66). Mutations that disrupt metal binding

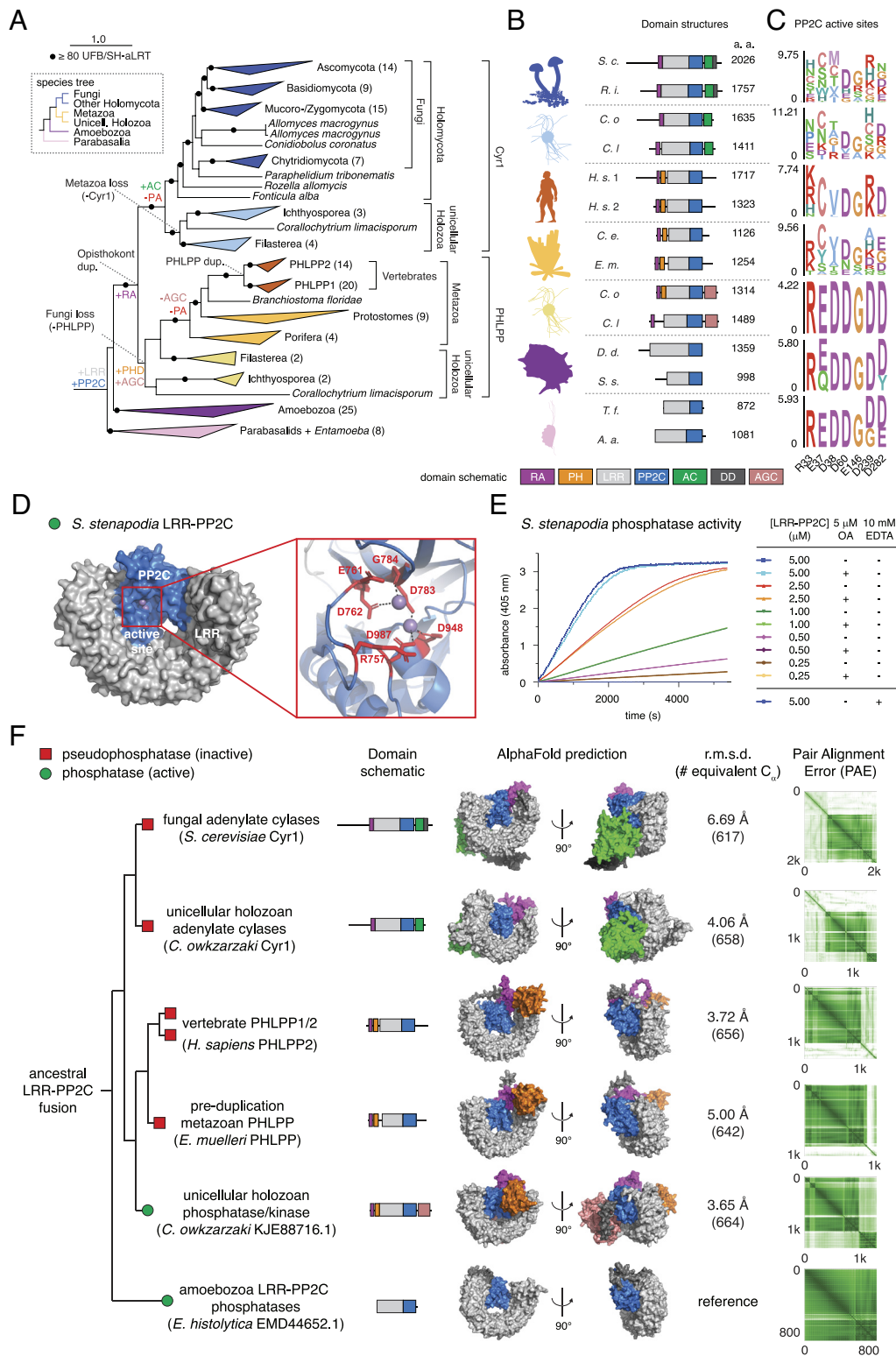


Fig. 6. Evolution and diversification of PHLPP genes. (A) Maximum-likelihood phylogeny of the LRR-PP2C protein family. Species and clade names have been added and the number of sequences within collapsed nodes are noted in parentheses. The gain and loss of genes, domains, and the PP2C active site (PA) have been mapped across the phylogeny based on Dollo parsimony. A species tree based on the phylogeny and current eukaryotic taxonomy (50) is shown for reference. The full phylogeny, domain annotations, and active site residues can be viewed at <https://itol.embl.de/shared/9pitR7NesER8>. (B) Representative domain architectures of proteins from across the LRR-PP2C phylogeny. Taxonomic groups are noted with cartoons obtained from Phylopic.org and protein lengths are shown in amino acids (a. a.). *S. c.*, *Saccharomyces cerevisiae*; *R. i.*, *Rhizophagus irregularis*; *C. o.*, *Capsaspora owkzarzaki*; *C. l.*, *Corallochytrium limacosporum*; *H. s. 1*, *Homo sapiens* PHLPP1; *H. s. 2*, *Homo sapiens* PHLPP2; *C. e.*, *Caenorhabditis elegans*; *E. m.*, *Ephydatia muelleri*; *D. d.*, *Dictyostelium discoideum*; *S. s.*, *Stenamoeba stenapodia*; *T. f.*, *Trithrichomonas foetus*; *A. a.*, *Anaeramoeba ignava*. RA, Ras binding domain; AC, adenylate cyclase; PH, PH-domain; DD, dimerization domain; LRR, leucine-rich repeat; AGC, AGC kinase domain; PP2C, PP2C domain. (C) Sequence logos showing PP2C active site conservation. PPM1A residues are noted for reference. (D) AlphaFold3 prediction of *S. stenapodia* LRR-PP2C. Inset: predicted coordination of M1 and M2 metal ions in the catalytic site. (E) Phosphatase activity of *S. stenapodia* LRR-PP2C against pNPP. (F) Domain architectures, AlphaFold2-predicted structures, and their associated confidence metrics (PAE plots). The rmsd of the LRR-PP2C domains (over C_{α} atoms) of each structure from the ancestral LRR-PP2C phosphatase of *Entamoeba histolytica* is shown for comparison. Red squares: pseudophosphatase (inactive); green circles: phosphatase (active).

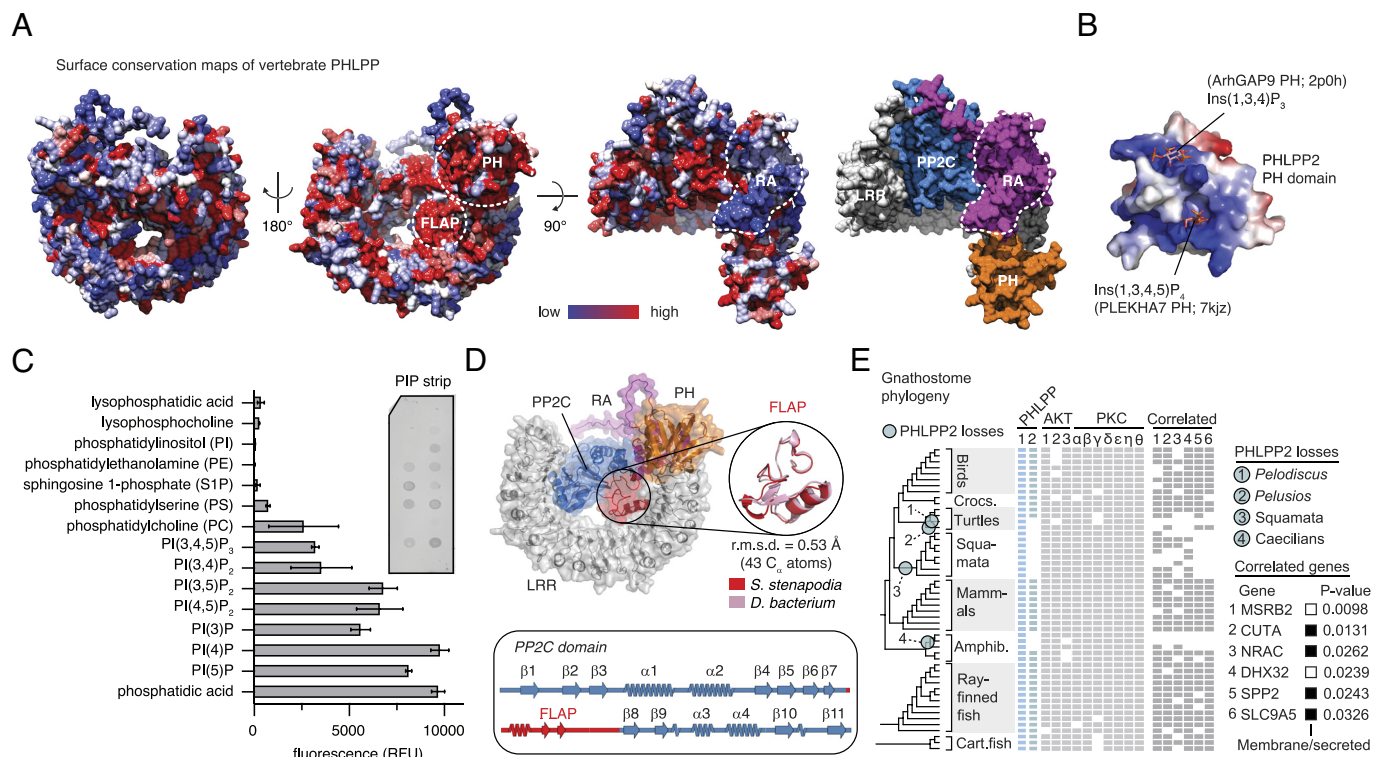


Fig. 7. PHLPP may have an alternative scaffolding role on membranes. (A) Surface conservation maps of vertebrate PHLPP. Low conservation (blue) to high conservation (red). Dashed white line: surface of the RA domain used to bind RAS in Cyt1. (B) Electrostatic surface potential map of the PH domain of *H. sapiens* PHLPP2. Phosphoinositide headgroup ligands superimposed from experimentally determined structures of homologous ArhGAP9 and PLEKHA7 PH domains identified by FoldSeek (65). (C) Lipid-protein overlay assay of PHLPP2 with phospholipids. Quantified signal is the mean of two independent replicates. (D) Conservation of the FLAP subdomain of the PHLPP PP2C domain. Secondary structure topology of the PP2C domain, indicating the FLAP subdomain in red. Circle *Inset*: superposition of AlphaFold-derived structures of FLAP-subdomain of *S. stenapodia* LRR-PP2C and a homologous PP2C phosphatase from the bacterium *Desulfobacterota bacterium*. (E) Phylogenomic profiling of gnathostomes to identify correlated gene presence and absence patterns for PHLPP2. Six of the most highly correlated genes are shown, alongside the presence/absence patterns of previously reported PHLPP2 substrates, Akt and PKC.

or divalent cations other than Mn^{2+} or Fe^{2+} (including Zn^{2+}) either abolish or strongly inhibit PPM1A activity (29, 67, 68). The observation of a single zinc ion in PHLPP2 with a complete coordination sphere suggests that PHLPP2 is incapable of canonical, binuclear-catalyzed phosphoester hydrolysis. Curiously, the carboxyl group of D822 in PHLPP2 occupies the same position as the phosphate group of a phosphorylated substrate peptide crystallized in complex with PPM1A (29), suggesting that loss of phosphatase activity may have coincided with a mutation that created a high-affinity zinc-binding site. Reports of pharmacologically active small molecule inhibitors of PHLPP should therefore be treated cautiously (15, 17). Since all known metal-dependent phosphatases of the PPM family, including ancient PPM homologs in cyanobacteria, depend on two or three divalent cations in their active sites for catalysis (69), the lack of phosphatase activity of PHLPP2 and the related PPM family pseudophosphatase TAB1 (33) is expected. On this basis, in fact, both PHLPP1 and PHLPP2 have previously been classified as pseudophosphatases (70). Although not explicitly tested in this study, the predicted loss of activity in the last common ancestor of metazoans implies that PHLPP1 is also a pseudophosphatase. This raises the obvious question of what function PHLPP fulfills in the cell.

Evidence Does Not Support a Role of PHLPP1 and PHLPP2 in Cancer. Conceptually, a tumor suppressive function of PHLPP follows logically from its identification as an Akt phosphatase. However, the lack of detectable phosphatase activity *in vitro* does not support this role. Reports characterizing PHLPP as a tumor suppressor have relied heavily on correlations between PHLPP expression levels and

Akt phosphorylation in cancer cell lines (12, 13). Causation was originally inferred from observations that reintroduction of PHLPP into a glioblastoma cell line resulted in suppression of tumor growth (12). Knockdown of PHLPP2 in cells also resulted in a significant increase in Akt S473 phosphorylation, which was interpreted to be a direct consequence of the loss of phosphatase activity (13). In the context of our findings, however, some of the previously reported effects on Akt phosphorylation may have been a pleiotropic effect of the ectopic overexpression of PHLPP. In particular, dominant negative effects on membrane signaling cannot be ruled out given the binding of PHLPP to phosphoinositides. However, a recent study revealed that adipose tissue-specific ablation of PHLPP2 in mice as well as siRNA-mediated knockdown of PHLPP2 in 3T3-L1 adipocytes did not lead to any significant differences in Akt S473 phosphorylation (71), suggesting that PHLPP2 may not be involved in Akt signaling, even indirectly.

Oncogenes and tumor suppressor genes have been carefully curated in the Cancer Gene Census, regularly updated by the COSMIC curation team (35). This list, which now numbers more than 700 human genes, requires indisputable mutation patterns in specific cancers reported in at least two independent studies from different groups. Consistent with the lack of somatic mutations in cancer, background mutation rates comparable to olfactory receptor genes, and no patterns of copy number loss in cancer, neither PHLPP1 nor PHLPP2 qualifies as a tumor suppressor. This contrasts starkly with Akt, which is a comprehensively validated oncogene. Taken together with the observation that PHLPP2 is a pseudophosphatase, the proposed role of PHLPP in cancer deserves further scrutiny, with an emphasis on its noncatalytic functions.

PHLPP Evolved from an Ancestral Phosphatase. The evolution of PHLPP from an ancestral phosphatase into two structurally homologous, but possibly functionally unrelated proteins is an example of neo- and subfunctionalization of a protein scaffold. The acquisition of an RA domain early in evolution implies that ancestral homologs of PHLPP were once able to bind RAS, but later lost this ability, supported by the absence of PHLPP in the proximal interactome of human RAS proteins (72). It seems highly probable that the RA domain was retained, despite loss of RAS binding, due to the intimate contacts it makes between the PP2C and LRR domains. The loss of RAS binding coincides with the acquisition of a PH domain that binds phosphoinositides, presumably substituting RAS interaction with direct membrane binding as a means of membrane localization. In principle, this should narrow the search for components of whatever biological pathway PHLPP is involved in. That pathway, however, is unlikely to involve AC, since this was an adaptation in the paralogous gene family to PHLPP. Although CAP is highly conserved in vertebrates, including its N terminus, there is no evidence of any structural homolog of the CTD of Cyr1 in animals (65). Whatever PHLPP interacts with, it is most likely mediated by the highly conserved FLAP subdomain of its phosphatase domain, an insert in PP2C family phosphatases with a well-characterized role in substrate binding. It is curious that genes that have been lost coincidentally with PHLPP2 are predominantly plasma membrane or secreted proteins. Coupled with the preferential binding of PHLPP2 to PI(4)P, a marker of the secretory pathway, a scaffolding role on a membrane-bound subcompartment seems plausible. However, this will undoubtedly require further investigation in a cellular context.

Finally, it should be noted that PHLPP1 was originally identified and annotated as suprachiasmatic nucleus (SCN) circadian oscillatory protein (SCOP), on account of the circadian pattern of its gene expression in the SCN (73). SCOP was later proposed to play a role in the regulation of mitogen-activated protein kinase (MAPK) signaling and memory formation in the hippocampus (74). These data, in combination with the possible ancestral connection between PHLPP and AGC kinases, implied by the presence of a kinase domain in early PHLPP homologs, could suggest that PHLPP regulates kinases through noncatalytic mechanisms or may participate in vestigial nonfunctional kinase interactions.

In summary, PHLPP is a pseudophosphatase. Public cancer repositories and genome-wide datasets provide no evidence for a role of either PHLPP1 or PHLPP2 in cancer. Phylogenetic and biochemical analyses indicate that the ancestral gene that gave rise to PHLPP was a bona fide phosphatase, but that this activity was lost early in evolution. Although genetic ablation of either or both genes in mice is not lethal and results in no reported predisposition to cancer, an evolutionary pressure of some sort has retained both PHLPP1 and PHLPP2 in vertebrates. Efforts to determine the biological pathways that PHLPP participates in will undoubtedly require a focus on its tissue expression patterns, subcellular localization, and interactome. Many clues almost certainly lie in its evolution.

Materials and Methods

Protein Expression and Purification. Recombinant human PHLPP2 and *S. stenopodia* LRR-PP2C were expressed as N-terminal GST fusion proteins in baculovirus-infected *Spodoptera frugiperda* (Sf9) cells and purified to homogeneity using affinity, ion-exchange, and size-exclusion chromatography. Details of the buffers can be found in *SI Appendix*.

Electron Microscopy. Purified, recombinant PHLPP2 samples were diluted to a final concentration of 50 µg/mL in spraying buffer containing 100 mM ammonium acetate and 30% (v/v) glycerol, pH 7.4. After dilution, the samples

were sprayed onto freshly cleaved mica chips and immediately transferred into a BAL-TEC MED020 high-vacuum evaporator equipped with electron guns. While rotating, the samples were coated with 0.7 nm platinum at an angle of 4 to 5°, followed by 10 nm carbon at 90°. The obtained replicas were floated off the mica chips and picked up on 400 mesh Cu/Pd grids. Grids were inspected in an FEI Morgagni 286D transmission electron microscope operated at 80 kV. Electron micrographs were acquired using an 11-megapixel Morada CCD camera from Olympus-SIS. Detailed methods for the preparation of samples for cryoelectron microscopy and image analysis can be found in *SI Appendix*.

MGA. MGAs were carried out according to the protocol of the Serine/Threonine Phosphatase Assay System (Promega). Serial dilutions of purified PHLPP2 or PP2A were incubated with 400 nM phospho-AL peptide (GATMKpTFCGT) or phospho-HM peptide (HFQpSYSAS) (GenScript) in the presence or absence of 12.5 nM okadaic acid for 1 h at 25 °C. For PHLPP2 immunoprecipitated from HEK293 cells, serial dilutions (five times 1:3 and one 1:10) were prepared in a 96-well plate. The samples were split into two groups, with one group supplemented with okadaic acid to a final concentration of 12.5 nM. All samples were combined with phosphorylated Akt1 activation loop peptide to a final concentration of 0.4 mM. Phosphate production was measured at 620 nm in a TECAN Spark® spectrofluorometer and converted into reaction rates (mol product/min) using a calibration curve derived from phosphate standards.

pNPP Phosphatase Assay. Serial dilutions of purified PHLPP2 or lambda phosphatase (purified in-house) were incubated with 10 mM pNPP in 20 mM Tris, pH 7.5, 150 mM KCl, 1 mM TCEP, and 2 mM MnCl₂ in the presence or absence of 12.5 nM okadaic acid for 1 h at 25 °C. For *S. stenopodia* LRR-PP2C, serial dilutions were incubated with 10 mM pNPP in 50 mM Tris, pH 7.5, 150 mM NaCl, 1 mM TCEP, and 0.1 mM MnCl₂ in the presence or absence of 5 µM okadaic acid or 10 mM EDTA at 25 °C. Absorbance at 405 nm was measured every 30 s for 90 min in a TECAN Spark spectrofluorometer.

Data, Materials, and Software Availability. Mass spectrometry data have been deposited in PRIDE; EMDB (PXD045891; PXD045978; PXD052551; EMDB-51182; EMDB-51183) (75–79).

ACKNOWLEDGMENTS. We thank M. Brandstetter and the Electron Microscopy Facility of the Vienna Biocenter Core Facilities (VBCF) for help collecting rotary-shadowed EM images of PHLPP2. We acknowledge Diamond for access and support of the cryo-EM facilities at the UK national electron Bio-Imaging Centre, proposal BI25222-3, as well as local contact Alistair Siebert for support. Proteomics analyses were performed by the Mass Spectrometry Facility at Max Perutz Labs using the VBCF instrument pool. This work was supported by Austrian Science Fund grants P33066, P36212, and W1261 as well as a Scientific and Technological Cooperation Grant (Austria-Bulgaria) of the Austrian Agency for Education and Internationalisation (BG 05/2023) to T.A.L. and a Bulgarian National Science Fund grant to T.D. (KP-06-Austria/1). K.M.S. was supported by an Austrian Academy of Sciences DOC PhD Fellowship. F.M.-S. was supported by the Austrian Science Fund doc.fund program (B-112). D.H. and the Haselbach lab are supported by Boehringer Ingelheim.

Author affiliations: ^aMax Perutz Labs, University of Vienna and Medical University of Vienna, Vienna 1030, Austria; ^bVienna BioCenter PhD Program, a Doctoral School of the University of Vienna and the Medical University of Vienna, Vienna A-1030, Austria; ^cResearch Institute of Molecular Pathology, Vienna BioCenter, Vienna 1030, Austria; ^dInstitute of Optical Materials and Technologies "Acad. J. Malinowski", Bulgarian Academy of Sciences, Sofia 1113, Bulgaria; ^eUniversity of Chemical Technology and Metallurgy, Sofia 1756, Bulgaria; ^fDepartment of Chemistry, Institute of Analytical Chemistry, University of Natural Resources and Life Sciences, Vienna 1190, Austria; ^gDepartment of Structural and Computational Biology, Center for Molecular Biology, University of Vienna, Vienna 1030, Austria; ^hMax Perutz Labs, Mass Spectrometry Facility, Vienna BioCenter Campus, Vienna 1030, Austria; ⁱDepartment of Biochemistry and Cell Biology, Center for Molecular Biology, University of Vienna, Vienna 1030, Austria; ^jDepartment of Microbiology, Immunobiology and Genetics, Center for Molecular Biology, University of Vienna, Vienna 1030, Austria; ^kResearch Center for Molecular Medicine, Austrian Academy of Sciences, Vienna 1090, Austria; ^lCenter for Medical Data Science, Institute of Artificial Intelligence, Medical University of Vienna, Vienna 1090, Austria; ^mFaculty of Chemistry and Pharmacy, Sofia University "St. Kliment Ohridski", Sofia 1164, Bulgaria; and ⁿGregor Mendel Institute, Austrian Academy of Sciences, Vienna BioCenter, Vienna 1030, Austria

1. K. M. Siess, T. A. Leonard, Lipid-dependent Akt-ivity: Where, when, and how. *Biochem. Soc. Trans.* **47**, 897–908 (2019).
2. B. D. Manning, A. Toker, AKT/PKB signaling: Navigating the network. *Cell* **169**, 381–405 (2017).
3. D. A. Fruman *et al.*, The PI3K pathway in human disease. *Cell* **170**, 605–635 (2017).
4. J. D. Carpten *et al.*, A transforming mutation in the pleckstrin homology domain of AKT1 in cancer. *Nature* **448**, 439–444 (2007).
5. M. J. Lindhurst *et al.*, A mosaic activating mutation in AKT1 associated with the Proteus syndrome. *N. Engl. J. Med.* **365**, 611–619 (2011).
6. D. Stokoe *et al.*, Dual role of phosphatidylinositol-3,4,5-trisphosphate in the activation of protein kinase B. *Science* **277**, 567–570 (1997).
7. D. D. Sarbassov, D. A. Guertin, S. M. Ali, D. M. Sabatini, Phosphorylation and regulation of Akt/PKB by the rictor-mTOR complex. *Science* **307**, 1098–1101 (2005).
8. W. J. Oh *et al.*, mTORC2 can associate with ribosomes to promote cotranslational phosphorylation and stability of nascent Akt polypeptide. *EMBO J.* **29**, 3939–3951 (2010).
9. J. Yang *et al.*, Crystal structure of an activated Akt/Protein Kinase B ternary complex with GSK3-peptide and AMP-PNP. *Nat. Struct. Biol.* **9**, 940–944 (2002).
10. Y.-C. Kuo *et al.*, Regulation of phosphorylation of Thr-308 of Akt, cell proliferation, and survival by the B55alpha regulatory subunit targeting of the protein phosphatase 2A holoenzyme to Akt. *J. Biol. Chem.* **283**, 1882–1892 (2008).
11. S. Padmanabhan *et al.*, A PP2A regulatory subunit regulates C. elegans insulin/IGF-1 signaling by modulating AKT-1 phosphorylation. *Cell* **136**, 939–951 (2009).
12. T. Gao, F. Furnari, A. C. Newton, PHLPP: A phosphatase that directly dephosphorylates Akt, promotes apoptosis, and suppresses tumor growth. *Mol. Cell* **18**, 13–24 (2005).
13. J. Brognard, E. Sieracki, T. Gao, A. C. Newton, PHLPP and a second isoform, PHLPP2, differentially attenuate the amplitude of Akt signaling by regulating distinct Akt isoforms. *Mol. Cell* **25**, 917–931 (2007).
14. Y.-A. Wen *et al.*, Loss of PHLPP protects against colitis by inhibiting intestinal epithelial cell apoptosis. *Biochim. Biophys. Acta* **1852**, 2013–2023 (2015).
15. D. G. Nowak *et al.*, The PHLPP2 phosphatase is a druggable driver of prostate cancer progression. *J. Cell Biol.* **218**, 1943–1957 (2019).
16. M. Chen *et al.*, Identification of PHLPP1 as a tumor suppressor reveals the role of feedback activation in PTEN-mutant prostate cancer progression. *Cancer Cell* **20**, 173–186 (2011).
17. E. Sieracki, W. Sinko, J. A. McCammon, A. C. Newton, Discovery of small molecule inhibitors of the PH domain leucine-rich repeat protein phosphatase (PHLPP) by chemical and virtual screening. *J. Med. Chem.* **53**, 6899–6911 (2010).
18. E. Sieracki, A. C. Newton, Biochemical characterization of the phosphatase domain of the tumor suppressor PH domain leucine-rich repeat protein phosphatase. *Biochemistry* **53**, 3971–3981 (2014).
19. K. Tachibana *et al.*, Okadaic acid, a cytotoxic polyether from two marine sponges of the genus Halichondria. *J. Am. Chem. Soc.* **103**, 2469–2471 (1981).
20. Y. Xing *et al.*, Structure of protein phosphatase 2A core enzyme bound to tumor-inducing toxins. *Cell* **127**, 341–353 (2006).
21. M. Andjelković *et al.*, Activation and phosphorylation of a pleckstrin homology domain containing protein kinase (RAC-PK/PKB) promoted by serum and protein phosphatase inhibitors. *Proc. Natl. Acad. Sci. U.S.A.* **93**, 5699–5704 (1996).
22. L. Truebestein *et al.*, Structure of autoinhibited Akt1 reveals mechanism of PIP3-mediated activation. *Proc. Natl. Acad. Sci. U.S.A.* **118**, e2101496118 (2021).
23. A. Brunet *et al.*, Akt promotes cell survival by phosphorylating and inhibiting a Forkhead transcription factor. *Cell* **96**, 857–868 (1999).
24. L. Santini *et al.*, FoxO transcription factors actuate the formative pluripotency specific gene expression programme. *Nat. Commun.* **15**, 7879 (2024).
25. D.-J. Shin *et al.*, Genome-wide analysis of FoxO1 binding in hepatic chromatin: Potential involvement of FoxO1 in linking retinoid signaling to hepatic gluconeogenesis. *Nucleic Acids Res.* **40**, 11499–11509 (2012).
26. B. L. Brauer *et al.*, Affinity-based profiling of endogenous phosphoprotein phosphatases by mass spectrometry. *Nat. Protoc.* **16**, 4919–4943 (2021).
27. M. Y. Hein *et al.*, A human interactome in three quantitative dimensions organized by stoichiometries and abundances. *Cell* **163**, 712–723 (2015).
28. W. C. Voegtli, D. J. White, N. J. Reiter, F. Rusnak, A. C. Rosenzweig, Structure of the bacteriophage lambda Ser/Thr protein phosphatase with sulfate ion bound in two coordination modes. *Biochemistry* **39**, 15365–15374 (2000).
29. S. Debnath *et al.*, A trapped human PPM1A-phosphopeptide complex reveals structural features critical for regulation of PPM protein phosphatase activity. *J. Biol. Chem.* **293**, 7993–8008 (2018).
30. A. K. Das, N. R. Helps, P. T. Cohen, D. Barford, Crystal structure of the protein serine/threonine phosphatase 2C at 2.0 Å resolution. *EMBO J.* **15**, 6798–6809 (1996).
31. K. Tanoue *et al.*, Binding of a third metal ion by the human phosphatases PP2Cα and Wip1 is required for phosphatase activity. *Biochemistry* **52**, 5830–5843 (2013).
32. G. Chen *et al.*, α-Klotho is a non-enzymatic molecular scaffold for FGF23 hormone signalling. *Nature* **553**, 461–466 (2018).
33. S. H. Conner *et al.*, TAK1-binding protein 1 is a pseudophosphatase. *Biochem. J.* **399**, 427–434 (2006).
34. L. W. Chung *et al.*, The ONIOM method and its applications. *Chem. Rev.* **115**, 5678–5796 (2015).
35. Z. Sondka *et al.*, The COSMIC Cancer Gene Census: Describing genetic dysfunction across all human cancers. *Nat. Rev. Cancer* **18**, 696–705 (2018).
36. Z. Sondka *et al.*, COSMIC: A curated database of somatic variants and clinical data for cancer. *Nucleic Acids Res.* **52**, D1210–D1217 (2024).
37. J. M. Dempster *et al.*, Chronos: A cell population dynamics model of CRISPR experiments that improves inference of gene fitness effects. *Genome Biol.* **22**, 343 (2021).
38. C. Pacini *et al.*, Integrated cross-study datasets of genetic dependencies in cancer. *Nat. Commun.* **12**, 1661 (2021).
39. R. M. Meyers *et al.*, Computational correction of copy number effect improves specificity of CRISPR-Cas9 essentiality screens in cancer cells. *Nat. Genet.* **49**, 1779–1784 (2017).
40. J. M. Dempster *et al.*, Extracting biological insights from the project Achilles genome-scale CRISPR screens in cancer cell lines. *bioRxiv* [Preprint] (2019). <https://doi.org/10.1101/720243>. Accessed 2024.
41. A. Tsherniak *et al.*, Defining a cancer dependency map. *Cell* **170**, 564–576.e16 (2017).
42. E. R. McDonald III *et al.*, Project DRIVE: A compendium of cancer dependencies and synthetic lethal relationships uncovered by large-scale, deep RNAi screening. *Cell* **170**, 577–592.e10 (2017).
43. R. Marcotte *et al.*, Functional genomic landscape of human breast cancer drivers, vulnerabilities, and resistance. *Cell* **164**, 293–309 (2016).
44. J. M. McFarland *et al.*, Improved estimation of cancer dependencies from large-scale RNAi screens using model-based normalization and data integration. *Nat. Commun.* **9**, 4610 (2018).
45. S. Miyamoto *et al.*, PHLP-1 negatively regulates Akt activity and survival in the heart. *Circ. Res.* **107**, 476–484 (2010).
46. B. Chen, J. A. Van Winkle, P. D. Lyden, J. H. Brown, N. H. Purcell, PHLP1 gene deletion protects the brain from ischemic injury. *J. Cereb. Blood Flow Metab.* **33**, 196–204 (2013).
47. D. V. Conti *et al.*, Trans-ancestry genome-wide association meta-analysis of prostate cancer identifies new susceptibility loci and informs genetic risk prediction. *Nat. Genet.* **53**, 65–75 (2021).
48. F. R. Schumacher *et al.*, Association analyses of more than 140,000 men identify 63 new prostate cancer susceptibility loci. *Nat. Genet.* **50**, 928–936 (2018).
49. S. Srivatsa *et al.*, Discovery of synthetic lethal interactions from large-scale pan-cancer perturbation screens. *Nat. Commun.* **13**, 7748 (2022).
50. F. Burki, A. J. Roger, M. W. Brown, A. G. B. Simpson, The new tree of eukaryotes. *Trends Ecol. Evol.* **35**, 43–55 (2020).
51. I. Uno *et al.*, Reconstitution of the GTP-dependent adenylate cyclase from products of the yeast CYR1 and RAS2 genes in Escherichia coli. *Proc. Natl. Acad. Sci. U.S.A.* **82**, 7855–7859 (1985).
52. M. J. Smith *et al.*, Evolution of AF6-RAS association and its implications in mixed-lineage leukemia. *Nat. Commun.* **8**, 1099 (2017).
53. B. J. Eves *et al.*, Structures of RGL1 RAS-association domain in complex with KRAS and the oncogenic G12V mutant. *J. Mol. Biol.* **434**, 167527 (2022).
54. B. Khannanavar, V. Mehta, C. Qi, V. Korkhov, Structure and function of adenylyl cyclases, key enzymes in cellular signaling. *Curr. Opin. Struct. Biol.* **63**, 34–41 (2020).
55. Y. Kuroda, N. Suzuki, T. Kataoka, The effect of posttranslational modifications on the interaction of Ras2 with adenylyl cyclase. *Science* **259**, 683–686 (1993).
56. V. Mehta *et al.*, Structure of Mycobacterium tuberculosis Cya, an evolutionary ancestor of the mammalian membrane adenylyl cyclases. *Elife* **11**, e77032 (2022).
57. J. Field *et al.*, Cloning and characterization of CAP, the S. cerevisiae gene encoding the 70 kd adenylyl cyclase-associated protein. *Cell* **61**, 319–327 (1990).
58. Y. Nishida *et al.*, Coiled-coil interaction of N-terminal 36 residues of cyclase-associated protein with adenylyl cyclase is sufficient for its function in Saccharomyces cerevisiae ras pathway. *J. Biol. Chem.* **273**, 28019–28024 (1998).
59. T. Gao, J. Brognard, A. C. Newton, The phosphatase PHLPP controls the cellular levels of protein kinase C. *J. Biol. Chem.* **283**, 6300–6311 (2008).
60. A. E. Aleshin *et al.*, Structural basis for the association of PLEKHA7 with membrane-embedded phosphatidylinositol lipids. *Structure* **29**, 1029–1039.e3 (2021).
61. D. F. J. Ceccarelli *et al.*, Non-canonical interaction of phosphoinositides with pleckstrin homology domains of Tiam1 and ArhGAP9. *J. Biol. Chem.* **282**, 13864–13874 (2007).
62. K. E. Pullen *et al.*, An alternate conformation and a third metal in PstP/Ppp, the M. tuberculosis PP2C-Family Ser/Thr protein phosphatase. *Structure* **12**, 1947–1954 (2004).
63. S. Caban-Penix, K. Ho, Z. Yang, R. Baral, N. Bradshaw, Docking interactions determine substrate specificity of members of a widespread family of protein phosphatases. *J. Biol. Chem.* **300**, 107700 (2024).
64. D. Waschbüsch *et al.*, Structural basis for the specificity of PPM1H phosphatase for Rab GTPases. *EMBO Rep.* **22**, e52675 (2021).
65. M. van Kempen *et al.*, Fast and accurate protein structure search with Foldseek. *Nat. Biotechnol.* **42**, 243–246 (2024).
66. C. Pan *et al.*, The catalytic role of the M2 metal ion in PP2Cα. *Sci. Rep.* **5**, 8560 (2015).
67. C. C. Field, J. M. Denu, Kinetic analysis of human serine/threonine protein phosphatase 2Cα. *J. Biol. Chem.* **274**, 20336–20343 (1999).
68. C. Pan *et al.*, Cadmium is a potent inhibitor of PPM phosphatases and targets the M1 binding site. *Sci. Rep.* **3**, 2333 (2013).
69. Y. Shi, Serine/threonine phosphatases: Mechanism through structure. *Cell* **139**, 468–484 (2009).
70. M. J. Chen, J. E. Dixon, G. Manning, Genomics and evolution of protein phosphatases. *Sci. Signal.* **10**, eaag1796 (2017).
71. K. Kim *et al.*, Adipocyte PHLPP2 inhibition prevents obesity-induced fatty liver. *Nat. Commun.* **12**, 1822 (2021).
72. J. R. Kovalski *et al.*, The functional proximal proteome of oncogenic Ras includes mTORC2. *Mol. Cell* **73**, 830–844.e12 (2019).
73. K. Shimizu, M. Okada, A. Takano, K. Nagai, SCOP, a novel gene product expressed in a circadian manner in rat suprachiasmatic nucleus. *FEBS Lett.* **458**, 363–369 (1999).
74. K. Shimizu, T. Phan, I. M. Mansuy, D. R. Storm, Proteolytic degradation of SCOP in the hippocampus contributes to activation of MAP kinase and memory. *Cell* **128**, 1219–1229 (2007).
75. W. Chen, T. A. Leonard, PHLP2 is a pseudophosphatase that lost activity in the metazoan ancestor. Proteomics Identifications Database (PRIDE). <https://www.ebi.ac.uk/pride/archive/projects/PXD045891>. Accessed 4 October 2023.
76. W. Chen, T. A. Leonard, PHLP2 is a pseudophosphatase that lost activity in the metazoan ancestor. Proteomics Identifications Database (PRIDE). <https://www.ebi.ac.uk/pride/archive/projects/PXD045978>. Accessed 4 October 2023.
77. D. Anrather, T. A. Leonard, PHLP2 is a pseudophosphatase that lost activity in the metazoan ancestor. Proteomics Identifications Database (PRIDE). <https://www.ebi.ac.uk/pride/archive/projects/PXD052551>. Accessed 24 May 2024.
78. D. Haselbach, T. A. Leonard, PHLP2 is a pseudophosphatase that lost activity in the metazoan ancestor. Electron Microscopy Data Bank. <https://www.ebi.ac.uk/emdb/EMD-51182>. Accessed 28 July 2024.
79. D. Haselbach, T. A. Leonard, PHLP2 is a pseudophosphatase that lost activity in the metazoan ancestor. Electron Microscopy Data Bank. <https://www.ebi.ac.uk/emdb/EMD-51183>. Accessed 28 July 2024.